Parameterizing surface and internal tide scattering and breaking on supercritical topography: the one- and two-ridge cases

Jody M. Klymak, *

School of Earth and Ocean Sciences and Department of Physics, University of Victoria, Victoria, Canada

Maarten C. Buijsman

Department of Physics, University of New Orleans, New Orleans, LA, 70148, USA

Sonya Legg

Program in Atmosphere and Ocean Sciences, Princeton University, Princeton, NJ, 08544, USA

Robert Pinkel

Scripps Institution of Oceanography, University of California, San Diego, La Jolla CA, 98105, USA

* *Corresponding author address:* Jody Klymak, School of Earth and Ocean Science, University of Victoria, PO Box 3055 STN CSC, Victoria B.C. Canada, V8W 3P6

E-mail: jklymak@uvic.ca

ABSTRACT

A parameterization is presented for turbulence dissipation due to internal tides generated at and impinging upon topography steep enough to be "supercritical" with respect to the tide. The parameterization requires knowledge of the topography, stratification, and the remote forcing, either barotropic or baroclinic. Internal modes that are arrested at the crest of the topography are assumed to dissipate, and faster modes assumed to propagate away. The energy flux into each mode is predicted using a knife-edge topography that allows linear numerical solutions. The parameterization is tested using high-resolution two-dimensional numerical models of barotropic and internal tides impinging on an isolated ridge, and for the generation problem on a two-ridge system. The recipe is seen to work well compared to numerical simulations of isolated ridges, so long as the ridge has a slope steeper than twice the critical steepness. For less steeply sloped ridges, near-critical generation becomes more dominant. For the two-ridge case, the recipe works well when compared to numerical model runs with very thin ridges. However, as the ridges are widened, even by a small amount, the recipe does poorly in an unspecified manner, because the linear response at high modes becomes compromised as it interacts with the slopes.

1. Introduction

The fate of tidal energy in the deep ocean is still not fully understood, despite the expectation that it is important in driving the vertical mixing of heat into the abyss, and ultimately driving the global overturning circulation (Munk and Wunsch 1998). Approximately 1TW of energy is believed to be lost from the barotropic tide in the deep ocean, compared to 2 TW on shallow shelves. However the fate of that 1TW of energy is still unknown.

Experiments at sites where surface tides are converted to internal tides (Polzin et al. 1997; Rudnick et al. 2003) indicate modest local turbulence. At topography that is predominantly subcritical to the internal tides, like some mid-ocean spreading centers, it is estimated that perhaps 30% of the energy lost from the surface tide goes into local dissipation (St. Laurent and Nash 2004), though more recent theoretical estimates make that fraction more variable depending on the local forcing (Polzin 2009) and the Coriolis frequency (Nikurashin and Legg 2011). These theories probably need more testing. However, the fate of the rest of the energy, predominantly in low modes, is not well understood. Similarly, for abrupt topography typical of mid-ocean ridges, like Hawaii, the fraction of energy dissipated locally is expected to be modest, both from available observations (Klymak et al. 2006), and from a theory similar to the one in this paper (Klymak et al. 2010b). Except for the strongest forcing or shallowest topography, the local dissipation is expected to be less than 10% of the energy removed from the surface tide; the rest again radiates away as low modes.

The local fraction of dissipation, while small compared to the total barotropic energy converted to internal wave energy, is still spectacular. Observations near Hawaii show overturns exceeding 200 m height at the ridge crest (Levine and Boyd 2006; Aucan et al. 2006;

Klymak et al. 2008). These near-bottom "breakers" were shown to be dominated by trapped lee waves that are generated near the ridge crest during each tidal cycle, and then propagate past the moorings as the tide changes (Legg and Klymak 2008; Klymak et al. 2010b). This lee-wave mechanism seems to dominate dissipation at supercritical ridges, though the observational tests of this are still being carried out (Alford et al. 2011). This motivated us to create a parameterization that predicts the energy in these lee waves. In steady state, the lee waves size can be predicted by comparing the speed of the horizontally propagating internal modes to the speed of the flow at the crest of the obstacle (Klymak and Legg 2010), with the lee wave representing a critical mode such that $c_c \approx U_m$, where c_c is the deep-water speed of the critical mode, and U_m is the speed of the barotropic flow at the ridge crest. Noting that such waves set up quickly if the topography is supercritical (Klymak et al. 2010a), we used the arrested wave criteria in an oscillating flow to determine the critical vertical modes at the obstacle crest. Dissipation in these waves was determined by considering the energy put into the modes higher than the critical mode (i.e. the trapped slow modes) as determined from a knife-edge model (St. Laurent et al. 2003; Llewellyn Smith and Young 2003). The resulting recipe was tested versus numerical simulations (Klymak et al. 2010b, hereafter KLP10) with quite good effectiveness. However, the fraction of energy dissipated locally from such ridges remained quite low, with much of the energy radiating away.

Given that much of the energy escapes super-critical topography, the question arises as to where it goes. One possibility is scattering of the radiated low modes at remote topography. Here we consider the dissipation that can occur when incoming internal tides impinge on a steep isolated obstacle, as well as the dissipation occurring during barotropic tidal flow over a double ridge system. In doing so, we extend the KLP10 recipe for dissipation during barotropic tidal flow over a single steep ridge to include multiple ridges and incoming baroclinic tides. The extended recipe is applied to several test cases, for which it is evaluated by comparison with explicit numerical simulations. The incoming tide problem may have applications to observations south of Hawaii on the tides impacting the Line Islands Ridge, and similar systems. The two-ridge problem was specifically aimed at Luzon Strait on the east side of the South China Sea. Recent efforts have indicated that double ridge systems may have stronger dissipation under barotropic tidal forcing than single ridges, with estimates ranging from 10% in a two-dimensional system (Buijsman et al. 2012) to 40% from a coarse three-dimensional model (Alford et al. 2011). Testing this configuration seems warranted, though preliminary efforts indicate that the two-dimensional assumption in the recipe presented here may be too simple (Buijsman et al. 2012).

We start with a discussion of the numerical model we use to test our recipe with (section 2), and then describe the phenomenology we are trying to model (section 3). The recipe itself is described (section 4), and tested on a one-ridge topography and a two-ridge topography, using the two dimensional numerical model as the "truth". For both setups, the recipe uses a knife-edge model to generate internal tides (described in the appendices), so the effect of varying width is tested (section 5) before summarizing and discussing further caveats (section 6).

2. The numerical model

As in KLP10, the proposed dissipation recipe will be tested against two dimensional simulation using the MITgcm (Marshall et al. 1997). This model has been used for other two-dimensional wave-breaking problems (Legg and Adcroft 2003; Legg and Huijts 2006; Legg and Klymak 2008; Klymak et al. 2010a). Forcing was applied via velocity and density nudging at boundaries more than two mode-1 horizontal wavelengths from the topography. The model was run using the hydrostatic approximation for numerical efficiency; tests with the non-hydrostatic terms did not reveal substantively different responses for this particular scenario (Klymak and Legg 2010). The models all use Gaussian topography, defined as $h(x) = h_i \exp\left(-\frac{x^2}{\sigma^2}\right)$. For the idealized runs below, we use a constant initial stratification of $N_0 = 5.2 \times 10^{-3}$ s^{-1} in a total water depth of $H = 2000$ m, and a Coriolis frequency of $f = 10^{-4}$ s^{-1}. As noted in KLP10, the Coriolis frequency enters into the generation-dissipation problem, with more energy generated and dissipated for lower f, but that the barotropic recipe does very well across the range of f, so we did not vary f here.

The dissipation scheme employed in this model is described in Klymak and Legg (2010), and consists of applying a high vertical viscosity and diffusivity whenever there are density overturns due to breaking waves. The diffusivity is scaled by the size of the density overturns so that the energy loss ϵ is consistent with the Ozmidov scale L_o

$$\epsilon = L_O^2 N^3, \tag{1}$$

where N is the stratification after overturns have been removed by density sorting. From this we obtain a turbulent viscosity and diffusivity of $K_v = 0.2\epsilon/N^2$ or $K_v = 10^{-5}$ m^{2}s^{-1}, whichever is larger. The limitations of this scheme are that it does not account for shear-driven mixing, and it does not work well if the breaking internal waves are small compared to the vertical grid size. This scheme does a better job than a local Mellor-Yamada 2.0 scheme (Mellor and Yamada 1982), and constant viscosities (Legg and Klymak 2008) at yielding energetically consistent estimates of dissipation for the parameter regimes explored here.

3. Phenomenology

As with barotropic generation (discussed in detail in KLP10), the dissipation of an incoming tide from a Gaussian ridge is dominated by an arrested lee wave that forms during each phase of the tide that has strong flow (figure 1). For a given topography and stratification, the size of this wave and the turbulence it generates depend on the incoming tide. For a mode-1 internal tide this dependence is relatively straight forward (figure 1a–b), and similar to the barotropic case. A lee wave forms on each side of the ridge during alternating phases of the incoming tide, with slightly more dissipation on the side of the topography facing the incoming wave (figure 1b).

For a wavefield with more than one mode, the response depends on the relative phasing of the modes, complicating determining the dissipation a-priori (figure 1c–h). Even for just a mode-1 and mode-2 incoming wave, the phasing of the modes changes the response at the crest of the topography, and can vary the dissipation by almost a factor of 3. Lee waves still form every cycle, but their size depends on whether the flow is reinforced or interfered with at the crest of the ridge.

Of recent interest because of work in the South China Sea, the generation and resonance of a two-ridge system is also considered. The generation and dissipation problem is similarly complex. The dissipation can vary significantly for the same forcing depending on the distance the ridges are from one another (figure 2). As we show below, this has to do with whether the "beams" from the ridges constructively or destructively interfere with one another. However, as with the other supercritical topography cases, the dissipation is dominated by near-crest turbulence generated in breaking trapped lee waves, so the same approach as for a baroclinic incoming tide is suggested below.

4. Recipe and Tests

The new, more general, recipe has the same ingredients as the recipe for the barotropic case (KLP10): a theoretical generation model gives the rate that energy is generated or scattered into radiated modes, F_n, and then the modes that have slower deep-water phase speed (c_n) than a characteristic ridge-top speed (U_n. i.e. $c_n < U_n$) are assumed to dissipate. The function F_n was calculated from a linear knife-edge model following St. Laurent et al. (2003).

For a WKB-stretched ocean with depth H, constant stratification N, and a knife-edge ridge of height h (and ridge-top water depth $H - h$, see figure 3), we decompose the forcing and response into vertical modes that obey the eigenvalue problem

$$\frac{d^2\phi}{dz^2} + \frac{N^2}{c_e^2}\phi(z) = 0 \tag{2}$$

where it is found from the boundary conditions at the seafloor and surface ($d\phi/dz = 0$) that $c_e(m) = NH/m\pi$, $m = 1, 2...$, and

$$\phi_m(z) = \cos\left(\frac{\pi m z}{H}\right). \tag{3}$$

Suppose we have an isolated piece of topography with a tide coming in from the positive-x direction. We assume a forcing comprised of incoming vertical modes:

$$u_i = \mathcal{R}\left[\sum_{m=0}^{M} a_i(m)\phi_m(z)\ e^{i(k_m x+\omega t)}\right], \tag{4}$$

where $a_i(m)$ is the complex amplitude of each vertical mode with shape $\phi_m(z)$, k_m the horizontal wavenumber, and ω, the frequency of the tide. The horizontal wavenumber is determined by $k_m = \left(\omega^2 - f^2\right)^{1/2} / c_e(m)$. The horizontal phase and group speeds are related to the eigenspeeds by:

$$c_g = c_e \frac{\sqrt{\omega^2 - f^2}}{\omega} \tag{5}$$

$$c_p = c_e \frac{\omega}{\sqrt{\omega^2 - f^2}}. \tag{6}$$

The internal response to this forcing is assumed to be comprised of a transmitted internal wave signal and a reflected one:

$$u_t = \mathcal{R}\left[\sum_{m=1}^{M} a_t(m)\phi_m(z)\ e^{i(k_m x+\omega t)}\right] \tag{7}$$

$$u_r = \mathcal{R}\left[\sum_{m=1}^{M} a_r(m)\phi_m(z)\ e^{i(k_m x-\omega t)}\right]. \tag{8}$$

If we assume a knife-edge topography and a linear response, the amplitudes $a_t(m)$ and $a_r(m)$ can be determined by matching the velocities at the topography, so that $u = 0$ at depths deeper than the ridge crest ($z < -H + h$) and u and w are matched above the ridge crest ($z > -H + h$). This leads to a matrix that can be inverted for the modal amplitudes, $a_t(m)$ and $a_r(m)$, as described in the appendix. These modal amplitudes can be expressed as energy fluxes by the relation:

$$F_n = \frac{H^2}{n\pi} g(\omega) \frac{|a_n|^2}{2} \tag{9}$$

where $g(\omega)$ is

$$g(\omega) = \rho \frac{\left[\left(N^2 - \omega^2\right)\left(\omega^2 - f^2\right)\right]^{1/2}}{\omega}. \tag{10}$$

The recipe for the turbulence requires knowing for what values of m the modes are arrested by ridge-top velocities, and thus are trapped and dissipate as part of the lee waves. For the barotropic situation in KLP10 the ridge-top speed was simply given by the barotropic speed at the crest of the obstacle:

$$U_n = U_T \frac{H}{H-h} \tag{11}$$

where U_T is the deep-water barotropic tide, H the depth of the deep water, and h the height of the obstacle.

Such a simple scaling does not work for the baroclinic case, as should be readily apparent from the examples given above (figure 1 and 2); the phasing of the forcing and response matters, and must be taken into account when determining the trapped mode that will form the lee wave. In order to account for the response, we propose a modified recipe as follows.

First, presupposing that the critical mode is M, the cross-ridge velocity response at the top of the ridge(s) is calculated from the linear solution made up only of modes lower than or equal to M. i.e.

$$u_M(z,t) = \sum_{m=0}^{M} a_m \phi_m(z) e^{i(k_m x_o - \omega t)} \tag{12}$$

Here a_m is meant to represent the solution on either side of the ridge crest, so for our single-ridge example $a_m = a_t = a_i + a_r$.

Second, the velocity response is averaged for half a vertical wavelength of the critical mode, $\lambda_M = H/M$ over the crest of the sill, and the maximum taken over the tidal cycle:

$$U_M = \max\left(\langle u_M(z,t)\rangle_{z=-H+h}^{-H+h+\lambda_M}\right)_{tide} \tag{13}$$

The vertical scale to average over is chosen following Klymak et al. (2010a), where the size of the lee wave is shown to be on the order of half a vertical wavelength of the arrested mode. This half-wavelength-averaged velocity scale is re-calculated starting with the first mode and moving to higher modes until a mode M is found such that $c_M \leq U_M$. This mode, M, is the first arrested mode, where $c_M = c_e(M)$ is the eigenspeed of the M-th mode. Once we determine the first arrested mode, M, the dissipation is calculated as $D = \sum_{n=M}^{\infty} F_n$, where F_n is the rate that energy is predicted to be put into each mode.

So to summarize, we:

i. Determine the linear response due to the forcing represented by the modal amplitudes $a_i(n)$, and thus the coefficients $a_t(n), a_r(n)$ and the energy fluxes F_n.

ii. Iterate through all modes M, and smooth the response at the top of the sill by H/M, to determine a velocity scale at the top of the ridge U_M.

iii. The lowest mode with eigenspeed slower than the corresponding U_M (i.e. $c_M < U_M$) is chosen as the critical mode.

iv. The dissipation is the sum of the rate of energy input into modes M and higher: $D = \sum_{n=M}^{\infty} F_n$

a. Test 1: Scattering of Mode 1 or Mode 2 from an isolated ridge

The recipe requires the expected velocity profile at the top of the ridge. To start, we consider the scattering of an incoming internal tide from a single isolated ridge. The problem can be solved numerically using linear algebra in a manner analogous to the barotropic generation problem (St. Laurent et al. 2003, KLP10) and the scattering problem from a continental shelf (Chapman and Hendershott 1981; Klymak et al. 2011). If an incoming tide is specified by modal amplitudes d_m, then we can calculate the transmitted internal tide, a_m, and the reflected, b_n by assuming the velocities match above the ridge and are zero below the ridge. Details follow the above papers and are presented briefly in the Appendix. From this, we can construct the velocity profile at the top of the ridge.

We first illustrate the iterative procedure to determine the critical mode, as described above. An example velocity profile is considered for a ridge with $h/H = 0.61$, $N = 5.2 \times 10^{-3}\ \mathrm{s}^{-1}$, and incoming mode-1 tide of amplitude $d_1 = 0.2\ \mathrm{m\,s}^{-1}$. For these runs, supercritical ridges were used, with $\sigma = 10$ km. For all modes (figure 4, grey lines, which are the same in all the panels), the velocity has a very sharp maximum at the ridge crest, and then a zero crossing approximately 200 m above (the high-wavenumber oscillations are due to choosing a finite number of modes to represent the solutions). figure 4a shows what happens if we guess that the critical mode is $M = 4$. $c_4 = 0.84\ \mathrm{m\,s}^{-1}$ (thin dashed line), and the black curve is the solution composed of only the first four modes. The mean of this $M = 4$ curve for a wavelength above the ridge crest is much less than c_4, $U_4 = 0.04\ \mathrm{m\,s}^{-1}$ (black dashed line), so mode-4 is not "critical" and can propagate away from the ridge. Trying the procedure on higher modes shows that $M = 12$ is still too low, $M = 20$ is too high, but $M = 16$ is the first mode that is critical.

The same procedure applies if the incoming mode-1 tide is stronger in amplitude, with a corresponding drop in the critical mode as amplitude increases (figure 5). Similarly, the response for different ridge heights changes non monotonically as the ridge and the incoming mode shapes interfere (figure 6). However, in general, very tall ridges do not dissipate as much as shorter ridges because a large fraction of energy reflects as low mode-waves. This is in contrast to the situation for a barotropic flow over a ridge, where the flow is forced through the constriction, developing large velocities, and therefore turbulent velocities.

The dissipation predicted by the recipe (D_{Th}) agrees very well with a suite of two-dimensional numerical experiments (D_{model}, figure 7; see table 1 for parameter space) There does tend to be some over-estimation of the numerical model turbulence by the theory, though just by a small factor. The strongest dissipations are also somewhat poorly constrained, likely as much due to the difficulty in estimating the internal tide amplitudes in a strongly non-linear environment as to a problem with the recipe[1]. Low dissipations predicted by the knife-edge model start to be over-predicted significantly. This is because the numerical model's vertical resolution is too low to properly resolve the turbulence in the lee waves as their vertical scale approaches the model resolution. In all, the recipe above could perhaps be tuned slightly to make the predicted dissipation smaller, but given the relative naiveté of the recipe, such tuning is not particularly warranted.

b. Test 2: Barotropic generation and mode-1 scattering from an isolated ridge

If there is a piece of topography that interacts with a remote incoming low-mode tide and the local barotropic tide, the combination of internal wave scattering and generation can have a significant impact on the internal tide response. This has been recently pointed out by Kelly and Nash (2010). The effect shows up profoundly for isolated topography even in

[1]The model is forced by boundary nudging, and thus the response away from the boundary is hard to specify precisely, and must be estimated from the model state, rather than be known *a priori*

the simple linear model, as we discuss here. We then consider the effect on the dissipation.

Using the linear methods described in the appendix, we can consider the case of a barotropic tide with an incoming tide over an isolated knife edge. This system has an interesting set of interactions that depend strongly on the phase between the two tides when they impact the topography (figure 8). In all cases, the same amount of internal energy transmits past the ridge. However, the fraction of that energy that is in mode-1 changes with the phase between the two forcing waves: at zero phase, almost all the transmitted energy is mode-1, while at 180 degrees out of phase, that fraction drops to almost zero. The difference in the reflected energy is even more pronounced, with almost no energy reflected in the zero-phase difference case (figure 8a), and a substantial increase for the out-of-phase case (figure 8e). All of the transmitted/reflected asymmetry in fluxes is in mode-1, as high modes must match at the ridge crest by the boundary conditions there (i.e. the length of the black portions of the bars in figure 8 is the same in both directions).

The full response of this simple linear system is surprisingly complex as we can see if we hold the ridge height constant and vary the ratio of the baroclinic to barotropic forcing (v_1/V_0) and their phase (figure 9). The total transmitted energy flux is simply the linear sum of the flux created by the barotropic generation and the baroclinic flux, and does not change with phase between the two forcings (figure 9a). However, the modal content of the transmitted flux changes significantly, with less high-mode energy when $v_1 \approx V_0$, and the phase difference is low (figure 9b). This difference is because the individual modal responses of the two forcings are slightly different, and constructively or destructively interfere. It is interesting that the effects balance, to produce a constant transmitted flux as a function of phase difference. The reflected flux is much more variable, and can be much stronger (figure 9b and d) because of the strong interaction between the barotropic wave, the incoming mode-1 wave, and the reflected wave. It is a curious result of this system that the asymmetry in the strength of the internal response is all on the side of the obstacle impacted by the incoming internal tide.

Just as the high-mode linear response strongly depends on the phase of the barotropic and baroclinic forcing, so does the dissipation predicted by the recipe (figure 10, solid line). When the phase differences between the barotropic and baroclinic tides are closer to 180, the response has more high-mode energy, and thus more dissipation. This effect is seen in the numerical model dissipation (figure 10, symbols), which agree very well with the recipe dissipations. We ran the simulations over a range of forcings and found very good agreement between the recipe and the simulations (figure 11).

This mixed-forcing case, and the two that follow, indicate why the recipe needed to be more complicated than the barotropic-generation case discussed in KLP10. As soon as there are two different modes, there is no single characteristic speed at the ridge crest we can appeal to in order to determine criticality, because the response changes significantly with the phase of the forcings.

c. *Test 3: Scattering of a Mode 1 combined with a Mode 2 incoming tide from an isolated ridge*

The behavior can become even more complex if there is more than one internal mode in the incoming tide because the phasing of the information at the two tides now depends on depth, and thus the height of the ridge. As an example, consider the case of a mode-1 and mode-2 incoming tide, both tides having the same amplitude, so that the energy flux in mode-1 is twice that in mode-2. The results of applying the recipe are quite complex (figure 12), with different ridge heights having distinctly different responses. For instance, short ridges ($h/H = 0.2$) have a response that is 180 degrees out of phase with taller ridges because the high velocities are near the seafloor rather than near the surface (see below).

Testing the recipe in the numerical model yields promising results (figure 13). Just considering the case of a ridge with $h/H = 0.25$, and mode-1 and mode-2 incoming tides each with 0.3 $\mathrm{m\,s^{-1}}$, we see a similar relationship between the numerically determined dissipation and the theory.

The nulls and peaks as the phase of the internal tide changes can easily be understood from the location of strong flows in the interfering tides (figure 14). For the in-phase mode-1 and mode-2 incoming tide, the location of the ridge is almost a null in the tidal velocity (figure 14a), leading to a weak response. Conversely, when mode-1 and mode-2 are exactly out of phase, the ridge has a strong lobe of velocity (figure 14b), so much so that a lot of energy is reflected upstream (figure 14d) and strong dissipation is found at the ridge (figure 14f).

d. Test 4: Dissipation at a pair of ridges

The final application is for a pair of ridges, a problem motivated by the situation in Luzon Strait. The two-ridge generation problem is solved with a similar linear method (see the Appendix), and the turbulence diagnosed at each ridge as was done above for a single ridge. This diagnosis is then compared to numerical model runs.

Before discussing the turbulence, it is worth pointing out that this simplified system has some complex, but classifiable behavior. The most striking effect comes if $h_1/H + h_2/H > 1$; then there is a resonance when the ridge separation, Δx, approaches half a mode-1 horizontal wavelength $\Delta x/\lambda_1 = 0.5$. In this case, any characteristics emanating inward from the ridge crests are trapped between the ridges, leading to a standing wave pattern that self reinforces upon returning to the emanating ridge. The radiating flux becomes much greater than the radiating flux from just one ridge, and a lot of energy is trapped between the two ridges (figure 16), similar to so-called attractors (Echeverri et al. 2011). If the barotropic forcing is held constant then the internal flux will go infinite, though of course in a real system the finite energy in the barotropic tide tide would prevent this, even in the absence of dissipation. Two tall ridges also can have slightly weaker response than a single ridge if the two ridge tops line up in such a way that their tops are connected by a characteristic (figure 16e).

If the ridges are short enough that ($h_1/H + h_2/H < 1$), then the perfect resonance does not occur. However, there is still a peak in the response where the two ridges positively reinforce one another by having intersecting characteristics after a bounce, either on the seafloor or the sea surface (figure 16c). Mathematically the seafloor bounce occurs for $\Delta x/\lambda_1 = (h_2 + h_1)/2H$, and the surface bounce for $\Delta x/\lambda_1 = (2 - h_2 - h_1)/2H$. Again, a null occurs when a characteristic joins the two peaks (figure 16a, $\Delta x/\lambda_1 = (h_1 - h_2)/2H$, if $h_1 > h_2$).

The overall complexity of the system can be judged by considering a fixed ridge height for one of the ridges, $h_1/H = 0.6$, and varying the other ridge height h_2/H and ridge spacing x/λ_1 (figure 17). First, if ridge 2 is "shadowed" by ridge 1, then the response is just the same as a single-ridge of height h_1/H, i.e. when $h_2 < 0.6 - 2\Delta x/\lambda_1$. Peaks in the response occur when the ridge crests line up after an odd number of bounces from either the surface, the seafloor, or the side of the topography (dotted lines figure 17). As noted above, resonance occurs at $\Delta x/\lambda_1 = 0.5$ for $h_2/H > 1 - h_1/H$. Off this resonance, tall h_2 still traps the energy for a number of bounces before it radiates away, so energy builds up between the ridges, and there is an enhancement of radiation.

The numerical model tests of the dissipation recipe were run with two ridge heights, and a number of separations. For all the runs, $h_1/H = 0.6$. For half the runs, $h_2/H = 0.17$; this geometry is similar to the geometry of the Luzon Straits in WKB-stretched co-ordinates. Sixteen simulations were then made with the ridges separated by $\Delta x/\lambda_1 = 0.1, 0.26, 0.55$ and 0.63, and barotropic forcing of $U = 0.03, 0.3, 1.0$ and $2.0\ \mathrm{m\,s^{-1}}$. As before, total depth was $H = 2000$ m, and stratification is constant at $N = 5.2 \times 10^{-3}\ \mathrm{s^{-1}}$. A smaller set of runs was made with $h_1/H = 0.6$ and $h_2/H = 0.27$, and spacing $\Delta x/\lambda_1 = 0.2, 0.3, 0.43, 0.8$. These were run only at $U = 0.25\ \mathrm{m\,s^{-1}}$. Narrow ridges were used ($\sigma = 2$ km), though the importance of ridge width was tested below.

The recipe given here is to calculate the linear response, and then determine what portion of that response dissipates local to the topography. Of course, in so doing, the response of the topography itself is changed; i.e. if mode 10 is dissipated at the right-hand ridge, it never reaches the left hand ridge to create part of the response. This affects the high-mode response, and thus the amount of dissipation predicted, typically leading to an overestimate. To account for this, we run the linear model described above twice. The first time, we determine what the critical mode is at each ridge from the full solution. We then re-calculate the linear response, but do not allow the super-critical modes to be part of the solution at the other ridge. For the runs presented below, this tends to reduce the predicted dissipation by approximately a factor of two.

Again, the dissipation recipe does well in predicting the dissipation of the ridge system (figure 18) usually well within a factor of 2, over 3 orders of magnitude of turbulence. With a bit more scatter, the dissipation at the individual ridges is also relatively well predicted (figure 18d), with the exception of three of the left-hand ridges (squares). These three exceptions are from when the short ridge is sheltered from the internal tide by the taller ridge, so there is a lot of dissipation at the tall ridge (which is well-predicted) and relatively little at the short ridge. Thus the theory is working with a particularly poor guess at the how the wave field is modified by turbulence, and does a relatively poor job at predicting the dissipation at the smaller, inconsequential, ridge.

5. Varying Width

There are many caveats to a recipe like the one presented here, but perhaps the most important is the role of varying topographic slopes. As discussed in KLP10, the knife-edge approximation is really only very good if the width of the topography is narrow enough that $dh/dx > 2\alpha$, where α is the slope of internal tide rays. For gentler slopes, lee waves are no longer the dominant dissipative mechanism, with near-critical bores becoming more important, until the flow becomes sub-critical, after which the dissipation drops off sharply.

For the baroclinic incoming tide case discussed here, the same dependence on slope applies (figure 19). For super-critical slopes, the recipe does quite well as the lee-wave physics dominates the dissipation. As dh/dx is decreased below 2α (i.e. σ/σ_c increases, where σ is the ridge width, and σ_c the ridge width where $dh/dx = \alpha$) the dissipation in the model increases to a peak at $dh/dx \approx \alpha$, and thus the theory (D_{th}) underpredicts.

Similar infidelity in the model can be seen for the two-ridge case (figure 20). Here, the mismatch surprisingly reaches a factor of two for even a moderately wide ridge, and oscillates much less deterministically than the one-ridge case. Similarly confusing results were obtained for other geometries and forcings. As discussed below, we feel this indicates that significant care should be taken in applying this recipe in a complicated situation like a two-ridge system where the response at one generation site depends strongly on the result at another.

6. Summary and Discussion

In the above we have demonstrated that turbulence dissipation at super-critical isolated features due to a baroclinic wavefield is concentrated at the crest of the features, and takes the form of lee waves as we found for barotropic generation (Legg and Klymak 2008; Klymak et al. 2010b). The dissipation in these lee waves can be predicted with reasonable fidelity by considering the linear generation from a knife-edge, and then assuming that all modes that move slower than an appropriately constructed ridge-crest speed are arrested, and dissipate locally. The ridge-crest speed in this recipe is the mean speed half a wavelength above the ridge crest of the mode being presumed critical, and comprising of only the faster modes. In order to find the critical mode, we therefore must iterate this procedure through all the modes, but the linear model is relatively cheap, and this is easy to do on a desktop computer.

We tested this recipe on numerical simulations using an isolated ridge, with barotropic, mode-1, and mode-2 incoming waves. When these waves are combined, the dissipation response at the ridge changes significantly depending on the phase difference between the waves, and the recipe replicates this very well (figure 13). We also tested the recipe on a two-ridge system with barotropic forcing, with very good results if the ridges were very thin in the numerical model (figure 18), again with very good predictive ability.

The same caveats apply to this analysis as applied to the barotropic generation case. If the obstacles are too wide in the along-wave direction, such that the slope is not sufficiently supercritical ($dh/dx > 2\alpha$) dissipation starts to be much larger in the simulations than predicted by the knife-edge theory. The problem with widening ridges is worse, and not fully understood, for the two-ridge case. Two ridges interact to create the internal response. Even mild widening of the ridges appears to change the lee wave response significantly enough that the recipe can be off by over a factor of two, even if the ridges are still sufficiently supercritical. To us, this indicates that even more substantial caution should be used when applying this recipe to complicated bathymetry like a two-ridge system.

A host of other caveats should be borne in mind before applying this recipe. Topography with a lot of "medium-scale" roughness should be treated with caution as subsidiary lee waves can develop (Nash et al. 2007). Large regions of near-critical slope have a similar problem. The effects of three-dimensionality mean that applying this recipe to complicated topography will be suspect (Buijsman et al. 2012).

Finally, it is important to determine how significant the dissipation in this problem actually is. To consider this, we examine the response of changing the height of the ridge and the incoming mode-1 tidal amplitude (figure 21). As with the barotropic case, it requires quite strong tides to get the fraction of energy dissipated above 10% of the incoming energy flux (figure 21b). Indeed, for the scattering problem, it is difficult for more than 20% of the energy to leave mode-1 (not shown). For tall ridges, most of the mode-1 energy reflects as a mode-1 tide, whereas for short ridges, most transmits. The greatest high-mode scattering and dissipation occurs at $h/H \approx 1/3$.

These findings still leave open the question of what happens to most of the low-mode tidal energy that radiates from supercritical ridges. The supercritical scattering process does not seem very dissipative, nor very efficient at moving energy into higher modes. This leaves open the possibility that mode-1 waves move through the oceans basins relatively un-molested. As noted here and other efforts (Kelly and Nash 2010), remote mode-1 internal tides can interfere with the generation of mode-1 internal tides by the barotropic tide, leading to the complicated picture of an ocean full of mode-1 energy (i.e Cummins and Oey 1997; Ray and Cartwright 2001) that is constructively and destructively interfering with local mode-1 generation, and having a non-trivial pathway to turbulence. Turbulence pathways are likely smaller-scale rough topography, near-critical slopes, and dissipation in shallow water (where the turbulence will not drive deep-ocean mixing). This leads to the speculation that the low-mode internal tide needs to be treated as a basin-scale phenomena for which the response needs to be calculated for the whole basin, rather than as local generation problems, in a manner similar to the surface tide.

APPENDIX

7. More Scattering and generation problems from knife-edge topography

a. Scattering and generation from a single knife-edge

The knife edge problem of tidal generation (St. Laurent et al. 2003; Klymak et al. 2010b) can be readily extended to a more general case that also includes an incident wavefield radiating from off-ridge (figure 3). We solve the problem in a WKB stretched co-ordinate system, with constant stratification N, water depth H and ridge height h. A barotropic tide is imposed with $U = U_o \cos \omega t$. The resulting baroclinic flows are decomposed into vertical modes:

$$
\begin{aligned}
u_i &= \Re\left\{\sum_{n=1}^{N} d_n \cos(n\pi z) e^{i(k_n x+\omega t)}\right\} && \text{(A1)}\\
u_r &= \Re\left\{\sum_{n=1}^{N} b_n \cos(n\pi z) e^{i(-k_n x+\omega t)}\right\} && \text{(A2)}\\
u_t &= \Re\left\{\sum_{n=1}^{N} a_n \cos(n\pi z) e^{i(k_n x+\omega t)}\right\} && \text{(A3)}\\
w_i &= \Re\left\{\sum_{n=1}^{N} d_n \sin(n\pi z) e^{i(k_n x+\omega t)}\right\} && \text{(A4)}\\
w_r &= \Re\left\{-\sum_{n=1}^{N} b_n \sin(n\pi z) e^{i(-k_n x+\omega t)}\right\} && \text{(A5)}\\
w_t &= \Re\left\{\sum_{n=1}^{N} a_n \sin(n\pi z) e^{i(k_n x+\omega t)}\right\} && \text{(A6)}
\end{aligned}
$$

where $k_n = \alpha n\pi/H$ are the horizontal wavenumbers, and α is the internal tide propagation angle:

$$\alpha = \left|\frac{k}{m}\right| = \left(\frac{\omega^2 - f^2}{N^2 - \omega^2}\right)^{1/2}. \tag{A7}$$

Note that the modal amplitudes a_n, etc. are allowed to be complex in general. This allows the incoming baroclinic tide to have a different phase at the ridge than the barotropic tide, and for the different modes to have varying phase.

If we define $\gamma = (H-h)/H$, and we require that the wavefields are matched at the ridge, $x = 0$ so that we find:

$$u_t = u_i + u_r \qquad -1 \leq z/H \leq 0 \tag{A8}$$

$$0 = U + u_i + u_r \qquad -1 \leq z/H \leq -\gamma \tag{A9}$$

$$w_t = w_i + w_r \qquad -\gamma \leq z \leq 0 \tag{A10}$$

The first condition says that $a_n = b_n + d_n$. We find the modal amplitudes by Fourier expansion about $\cos m\pi z/H$ for $m = 0, 1, ..., N-1$, giving us N linear equations in N unknowns:

$$(A_{mn} + B_{mn})b_n + A_{mn}d_n = c_n \tag{A11}$$

where c_m is a column vector as in St. Laurent et al. (2003)

$$c_n = \frac{U_o}{n}\sin(n\pi\gamma) \tag{A12}$$

where $\gamma = (H-h)/H$, and $c_o = -U_o\pi(1-\gamma)$ for $m = 0, 1, ...N-1$. The matrices A and B are the two components of S03's A matrix:

$$A_{mn} = \frac{n\,\sin n\pi\gamma\;\cos m\pi\gamma - m\,\cos n\pi\gamma\;\sin m\pi\gamma}{m^2 - n^2} \tag{A13}$$

$$B_{mn} = \frac{n - n\,\cos n\pi\gamma\;\cos m\pi\gamma - m\,\sin n\pi\gamma\;\sin m\pi\gamma}{m^2 - n^2} \tag{A14}$$

and for the singularities

$$A_{mm} = \frac{m\pi(1-\gamma) - \sin m\pi\gamma \cos m\pi\gamma}{2m\pi} \tag{A15}$$

$$B_{mm} = \frac{-\sin^2 m\pi\gamma}{2m\pi} \tag{A16}$$

Note that the above reduces to S03's knife-edge when $d_n = 0$. Equation (A11) is easily inverted to solve for the vector b_n (so long as γ is not allowed to be too close to an integer division of 1, so instead of using $\gamma = 0.5$, we use $\gamma = 0.50001$, otherwise singularities result).

b. Generation from two knife-edges

The generation problem from two knife edges proceeds in a very similar manner. Here one ridge is supposed to be at $x = 0$ with height h_o and the other at $x = L$, with height h_L.

Again, we can divide the velocities into modes:

$$
\begin{aligned}
u_a &= U_o \sum_{n=1}^{N} a_n \cos(n\pi z) e^{i(k_n x + \omega t)} && \text{(A17)}\\
u_b &= U_o \sum_{n=1}^{N} b_n \cos(n\pi z) e^{i(-k_n x + \omega t)} && \text{(A18)}\\
u_c &= U_o \sum_{n=1}^{N} c_n \cos(n\pi z) e^{i(k_n x + \omega t)} && \text{(A19)}\\
u_d &= U_o \sum_{n=1}^{N} d_n \cos(n\pi z) e^{i(-k_n x + \omega t)} && \text{(A20)}\\
w_a &= U_o \sum_{n=1}^{N} a_n \sin(n\pi z) e^{i(k_n x + \omega t)} && \text{(A21)}\\
w_b &= -\alpha U_o \sum_{n=1}^{N} b_n \sin(n\pi z) e^{i(-k_n x + \omega t)} && \text{(A22)}\\
w_c &= \alpha U_o \sum_{n=1}^{N} c_n \sin(n\pi z) e^{i(k_n x + \omega t)} && \text{(A23)}\\
w_d &= -\alpha U_o \sum_{n=1}^{N} d_n \sin(n\pi z) e^{i(-k_n x + \omega t)} && \text{(A24)}
\end{aligned}
$$

where $k_n = \alpha n \pi$ are the horizontal wave numbers and the amplitudes are complex.

So, the matching conditions at $x = 0$ are as before:

$$
\begin{aligned}
u_a &= u_b + u_c \qquad -1 \le z \le 0 && \text{(A25)}\\
-1 &= u_b + u_c \qquad -1 \le z \le -\gamma_0 && \text{(A26)}\\
w_a &= w_b + w_c \qquad -\gamma_0 \le z \le 0 && \text{(A27)}
\end{aligned}
$$

At $x = L$ they are

$$
\begin{aligned}
u_d &= u_b + u_c \qquad -1 \le z \le 0 && \text{(A28)}\\
-1 &= u_b + u_c \qquad -1 \le z \le -\gamma_L && \text{(A29)}\\
w_d &= w_b + w_c \qquad -\gamma_L \le z \le 0 && \text{(A30)}
\end{aligned}
$$

The first implies that $a_n = b_n + c_n$. The second implies that $d_n e^{-ik_nL} = b_n e^{-ik_nL} + c_n e^{ik_nL}$. We will shorten $d_n e_n^- = b_n e_n^- + c_n e_n^+$. This eliminates a_n and d_n so we just need to solve for b_n and c_n.

$$-1 = \sum_{n=1}^{N}(b_n + c_n)C_n \quad z \le -\gamma_0 \tag{A31}$$

$$\sum_{n=1}^{N} a_n S_n = \sum_{n=1}^{N}(c_n - b_n)S_n \quad z \ge -\gamma_0 \tag{A32}$$

becomes

$$\sum_{n=1}^{N}(b_n + c_n)C_n = -1 \quad z \le -\gamma_0 \tag{A33}$$

$$\sum_{n=1}^{N} b_n S_n = 0 \quad z \ge -\gamma_0 \tag{A34}$$

Similarly at $x = L$:

$$\sum_{n=1}^{N}(e_n^- b_n + e_n^+ c_n)C_n = -1 \quad z \le -\gamma_L \tag{A35}$$

$$\sum_{n=1}^{N}(e_n^+ c_n)S_n = 0 \quad z \ge -\gamma_L \tag{A36}$$

Again integrating by $cos(m\pi z)$

$$(A_0 + B_0)b + A_0 c = C_0 \tag{A37}$$

$$(A_L + B_L)(E^+ c) + A_L(E^- b) = C_L, \tag{A38}$$

where the matrices A_L, A_0, B_L, B_0 are as in the previous section with the proper choice of γ. C_L is the same as c in the previous section, evaluated for $\gamma = \gamma_L$, and C_0 is for γ_o. The notation E^+, E^- are diagonal matrices that represent the phase shift between $x = L$ and

$x = 0$:

$$E^+_{mn} = \delta(m-n)exp(ik_nL) \tag{A39}$$

$$E^-_{mn} = \delta(m-n)exp(-ik_nL) \tag{A40}$$

$$\tag{A41}$$

Solving, we get

$$b = D_0^{-1}(C_0 - A_0c) \tag{A42}$$

$$(D_LE^+ - A_LE^-D_o^{-1}A_0)c = C_L - A_LE^-D_o^{-1}C_0 \tag{A43}$$

where the last equation is invertible to get c_n.

Acknowledgments.

Thanks to two anonymous reviewers for helpful comments and suggestions. This work was funded by the US Office of Naval Research under grants N00014-09-1-0274

REFERENCES

Alford, M. H., et al., 2011: Energy flux and dissipation in Luzon Strait: two tales of two ridges. *J. Phys. Oceanogr*, **41 (11)**, 2211–2222, doi:10.1175/JPO-D-11-073.1.

Aucan, J., M. A. Merrifield, D. S. Luther, and P. Flament, 2006: Tidal mixing events on the deep flanks of Kaena Ridge, Hawaii. *J. Phys. Oceanogr.*, **36**, 1202–1219.

Buijsman, M. C., S. Legg, and J. M. Klymak, 2012: Double ridge internal tide interference and its effect on dissipation in Luzon Strait. *J. Phys. Oceanogr*, **42**, 1337–1356.

Chapman, D. and M. Hendershott, 1981: Scattering of internal waves obliquely incident upon a step change in bottom relief. *Deep Sea Research Part A.*, **28 (11)**, 1323–1338.

Cummins, P. and L. Oey, 1997: Simulation of barotropic and baroclinic tides off northern british columbia. *Journal of Physical Oceanography*, **27 (5)**, 762–781.

Echeverri, P., T. Yokossi, N. Balmforth, and T. Peacock, 2011: Tidally generated internal-wave attractors between double ridges. *Journal of Fluid Mechanics*, **669**, 354–374.

Kelly, S. and J. Nash, 2010: Internal-tide generation and destruction by shoaling internal tides. *Geophysical Research Letters*, **37**, L23 611.

Klymak, J., M. Alford, R. Pinkel, R. Lien, Y. Yang, and T. Tang, 2011: The breaking and scattering of the internal tide on a continental slope. *J. Phys. Oceanogr*, **41**, 926–945, doi:10.1175/2010JPO4500.1.

Klymak, J. M., S. Legg, and R. Pinkel, 2010a: High-mode stationary waves in stratified flow over large obstacles. *J. Fluid Mech.*, **644**, 312–336.

Klymak, J. M., S. Legg, and R. Pinkel, 2010b: A simple parameterization of turbulent tidal mixing near supercritical topography. *J. Phys. Oceanogr.*, **40 (9)**, 2059–2074, doi:10.1175/2010JPO4396.1, `http://journals.ametsoc.org/doi/pdf/10.1175/2010JPO4396.1`.

Klymak, J. M. and S. M. Legg, 2010: A simple mixing scheme for models that resolve breaking internal waves. *Ocean Modell.*, **33 (3-4)**, 224 – 234, doi:10.1016/j.ocemod.2010.02.005.

Klymak, J. M., R. Pinkel, and L. Rainville, 2008: Direct breaking of the internal tide near topography: Kaena Ridge, Hawaii. *J. Phys. Oceanogr.*, **38**, 380–399.

Klymak, J. M., et al., 2006: An estimate of tidal energy lost to turbulence at the Hawaiian Ridge. *J. Phys. Oceanogr.*, **36**, 1148–1164.

Legg, S. and A. Adcroft, 2003: Internal wave breaking at concave and convex continental slopes. *J. Phys. Oceanogr.*, **33**, 2224–2246.

Legg, S. and K. M. Huijts, 2006: Preliminary simulations of internal waves and mixing generated by finite amplitude tidal flow over isolated topography. *Deep Sea Research Part II: Topical Studies in Oceanography*, **53 (1-2)**, 140 – 156, doi:DOI:10.1016/j.dsr2.2005.09.014.

Legg, S. and J. M. Klymak, 2008: Internal hydraulic jumps and overturning generated by tidal flow over a tall steep ridge. *J. Phys. Oceanogr.*, **38 (9)**, 1949–1964.

Levine, M. D. and T. J. Boyd, 2006: Tidally-forced internal waves and overturns observed on a slope: results from the HOME survey component. *J. Phys. Oceanogr.*, **36**, 1184–1201.

Llewellyn Smith, S. G. and W. R. Young, 2003: Tidal conversion at a very steep ridge. *J. Fluid Mech.*, **495**, 175–191.

Marshall, J., A. Adcroft, C. Hill, L. Perelman, and C. Heisey, 1997: A finite-volume, incompressible Navier-Stokes model for studies of the ocean on parallel computers. *J. Geophys. Res.*, **102 (C3)**, 5753–5766.

Mellor, G. L. and T. Yamada, 1982: Development of a turbulence closure model for geophysical fluid problems. *Rev. Geophys. Space Phys.*, **20**, 851–875.

Munk, W. and C. Wunsch, 1998: Abyssal recipes II: energetics of tidal and wind mixing. *Deep Sea Res.*, **45**, 1977–2010.

Nash, J., M. Alford, E. Kunze, K. Martini, and S. Kelley, 2007: Hotspots of deep ocean mixing on the Oregon continental slope. *Geophys. Res. Lett.*, **34**, L01 605, doi:10.1029/2006GL028 170.

Nikurashin, M. and S. Legg, 2011: A mechanism for local dissipation of internal tides generated at rough topography. *J. Phys. Oceanogr*, **41 (2)**, 378–395.

Polzin, K., J. Toole, J. Ledwell, and R. Schmitt, 1997: Spatial variability of turbulent mixing in the abyssal ocean. *Science*, **276**, 93–96.

Polzin, K. L., 2009: An abyssal recipe. *Ocean Modelling*, doi:doi:10.1016/j.ocemod.2009.07.007.

Ray, R. and D. Cartwright, 2001: Estimates of internal tide energy fluxes from TOPEX/Poseidon altimetry: Central North Pacific. *Geophys. Res. Lett.*, **28**, 1259–1262.

Rudnick, D. L., et al., 2003: From tides to mixing along the Hawaiian Ridge. *Science*, **301 (5631)**, 355–357.

St. Laurent, L. C. and J. D. Nash, 2004: An examination of the radiative and dissipative properties of deep ocean internal tides. *dsrii*, **51 (25-26)**, 3029 – 3042, doi:10.1016/j.dsr2.2004.09.008.

St. Laurent, L. C., S. Stringer, C. Garrett, and D. Perrault-Joncas, 2003: The generation of internal tides at abrupt topography. *Deep Sea Res. I*, **50**, 987–1003,10.1016/S0967–0637(03)00 096–7.

List of Tables

TABLE 1. Parameter matrix for numerical runs used in Case 1, monochromatic tide scattering from an isolated ridge. There were 24 runs in total, as summarized in FIG. 7. For all runs, $N = 5.2 \times 10^{-3}\ \mathrm{s}^{-1}$ and $f = 5.23 \times 10^{-5}\ \mathrm{s}^{-1}$, and $H = 2000\mathrm{m}$.

parameter	values
modes	1 and 2
h/H	0.75, 0.55, 0.25
$u_i(m)[\mathrm{ms}^{-1}]$	0.10, 0.25, 0.55, 1.00

TABLE 2. Parameter matrix for numerical runs used in Case 2, barotropic tide (v_0) and incoming baroclinic tide (v_1) combined. There were 32 runs in total, as summarized in FIG. 11. For all runs, $N = 5.2 \times 10^{-3}$ s^{-1} and $f = 5.23 \times 10^{-5}$ s^{-1}, $H = 2000$m, and $h/H = 0.6$. Each forcing was run with phase differences at the topography of 0, 45, 90, and 135 degrees.

$v_0[\mathrm{m\,s^{-1}}]$	$v_1[\mathrm{m\,s^{-1}}]$
0.025	0.15, 0.25
0.10	0.02, 0.05, 0.10, 0.25
0.20	0.15, 0.55

TABLE 3. Parameter matrix for numerical runs used in Case 3, mode-1 and mode-2 tides combined scattering from an isolated ridge. There were 24 runs in total, as summarized in FIG. 15. For all runs, $N = 5.2 \times 10^{-3}$ s^{-1} and $f = 5.23 \times 10^{-5}$ s^{-1}, and $H = 2000$m.

parameter	values
modes	1 and 2
h/H	0.75, 0.55, 0.25
$u_i(m)$[ms^{-1}]	0.10, 0.25, 0.55, 1.00

TABLE 4. Parameter matrix for numerical runs used in Case 4, barotropic tides generated at two ridges. There were 25 runs in total, as summarized in FIG. 15. For all runs, $N = 5.2 \times 10^{-3}$ s^{-1} and $f = 1.0 \times 10^{-4}$ s^{-1}, and $H = 2000$m. The left ridge has $h_l = 0.17$, and the right $h_r = 0.6$. The separation between the left and right ridges is scaled by the mode-1 wavelength: $\lambda_1 = 210$ km.

separation ($\Delta x/\lambda_1$)	V_0[ms^{-1}]
0.10	0.03, 0.30, 1.00, 2.00
0.22	0.03, 1.00
0.26	0.03, 0.30, 1.00, 2.00
0.30	0.03, 1.00
0.35	0.03, 1.00
0.38	0.03, 1.00
0.55	0.03, 0.30, 1.00, 2.00
0.63	0.03, 0.30, 1.00, 2.00
0.65	0.03

List of Figures

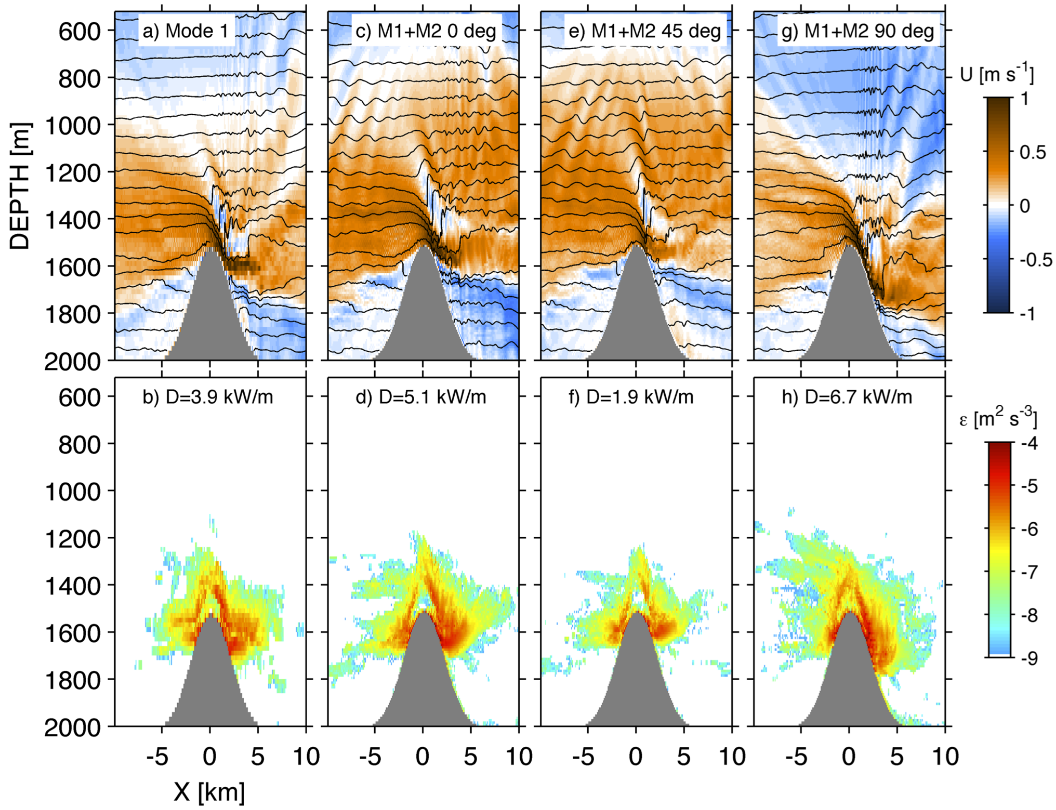

FIG. 1. Numerical model runs demonstrating the response of a Gaussian ridge to incoming internal tides. These runs all have a constant stratification $N = 5.2 \times 10^{-3}$ s^{-1}. a) velocity snapshot of a 0.55 m s^{-1} mode-1 incoming tide, impinging from the right. Contours are density. b) dissipation for the mode-1 tide, averaged for a tidal cycle. c–d) for a mode-1 and mode-2 tide with the same amplitudes and the same velocity phase at the sea surface above the topography. e–f) for a mode-1 and mode-2 tide with the same amplitudes, but 45 degree phase shift at the ridge. g–h) 90 degree phase shift at the ridge.

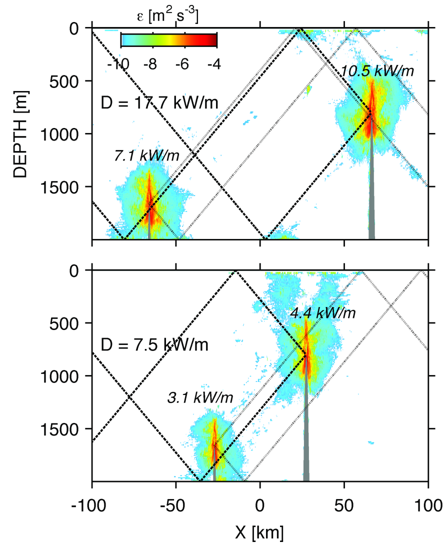

FIG. 2. Turbulence dissipation for the tidal generation problem of two ridges that are 0.6 and 0.17 of the water depth. For the upper panel, the tidal characteristics from the two ridges reinforce one another. For the lower, the up going ray from the small ridge works against the down going ray from the large ridge, reducing the response. An analytic model described in this paper captures this weak resonance.

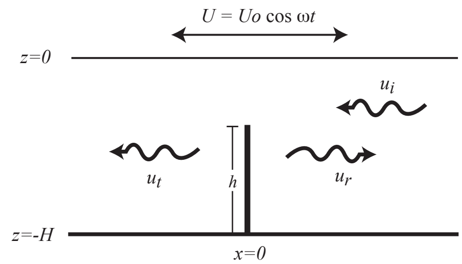

FIG. 3. Setup of the general one-ridge linear problem, including a barotropic tide, and an incoming internal wave from the right hand side.

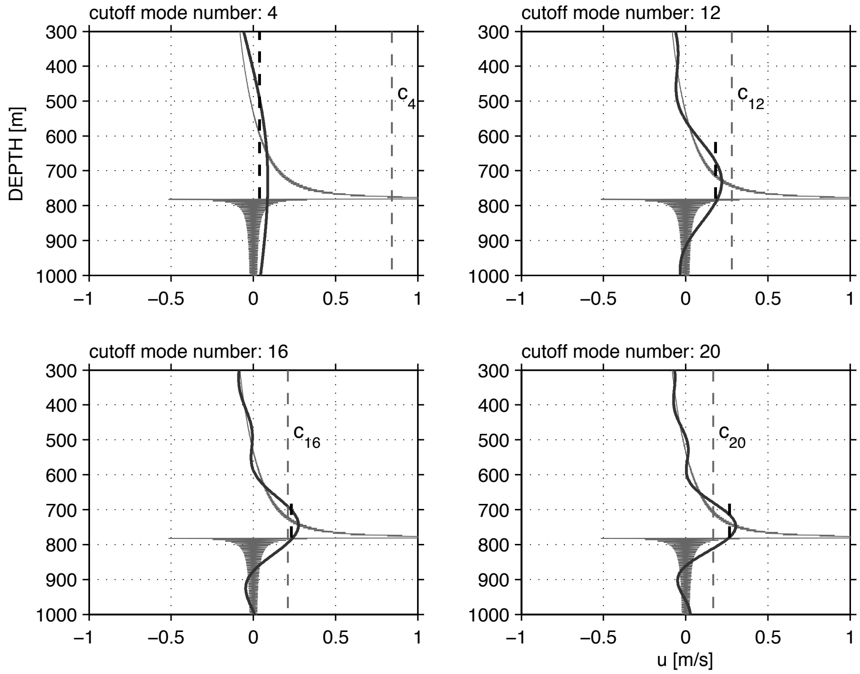

FIG. 4. Example iterations on choosing a critical mode using the generated response and the incoming forcing as input parameters. The response is for a mode-1 incoming wave. In all 4 panels, the thin line is the full modeled response. The black line is the smoothed velocity removing the modes higher than the mode being tested, and the black dashed line the mean speed over the half wavelength of the mode being tested; note that this scale gets smaller as the mode gets higher, corresponding to the expected lee wave getting smaller. The grey dashed line is the lateral phase speed of the mode being tested.

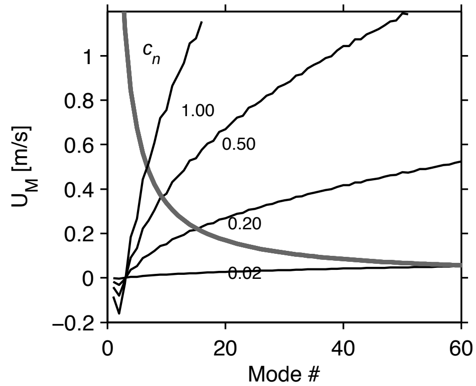

FIG. 5. Values of U_M for 4 values of the incoming mode-1 amplitude impacting a ridge with $h/H = 0.61$ ($N = 5.2 \times 10^{-3}$ s^{-1}, $H = 2000$ m). The thin lines are the speed at the top of the ridge assuming that the indicated mode is the critical one, as described in the text. This speed increases as mode number increases because the smoothing of the ridge-top velocity is less, so more of the near-ridge peak is part of the estimate (see FIG. 4). The speed of the each internal mode is indicated by the grey curve. Where the thin lines intersect the grey curve indicates the critical mode.

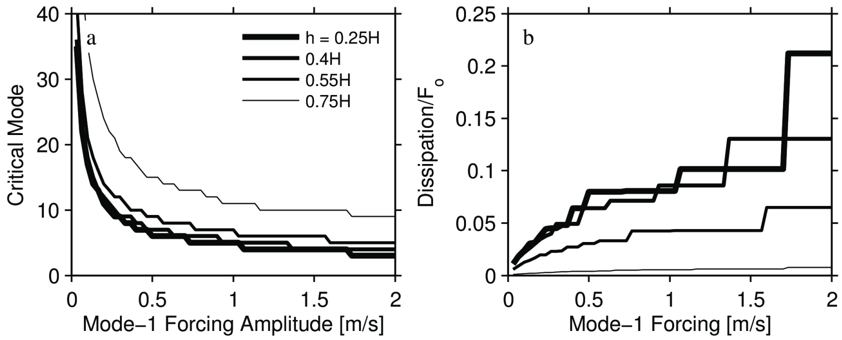

Fig. 6. a) Critical mode number for an incoming mode-1 tide of increasing amplitudes impacting on four different ridge heights. b) fraction of incoming mode-1 energy that is dissipated for different ridge heights as a function of forcing strength.

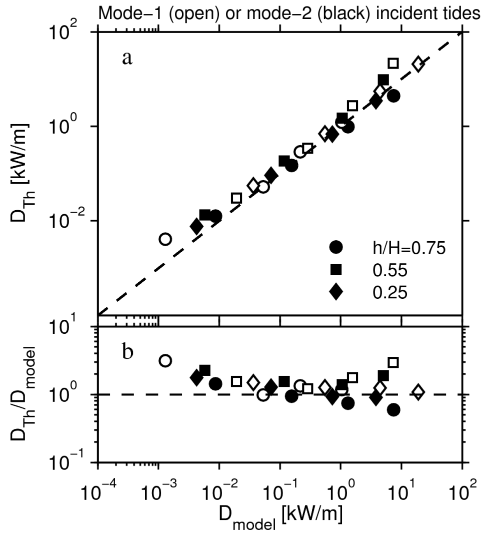

FIG. 7. Dissipation due to mode-1 (open symbols) or mode-2 (black) incoming internal tides impacting a thin Gaussian ridge in a numerical model (D_{model}) and due to the recipe presented here (D_{Th}). Different ridge heights are indicated by the shape of the symbols, and a number of different internal tide amplitudes were used.

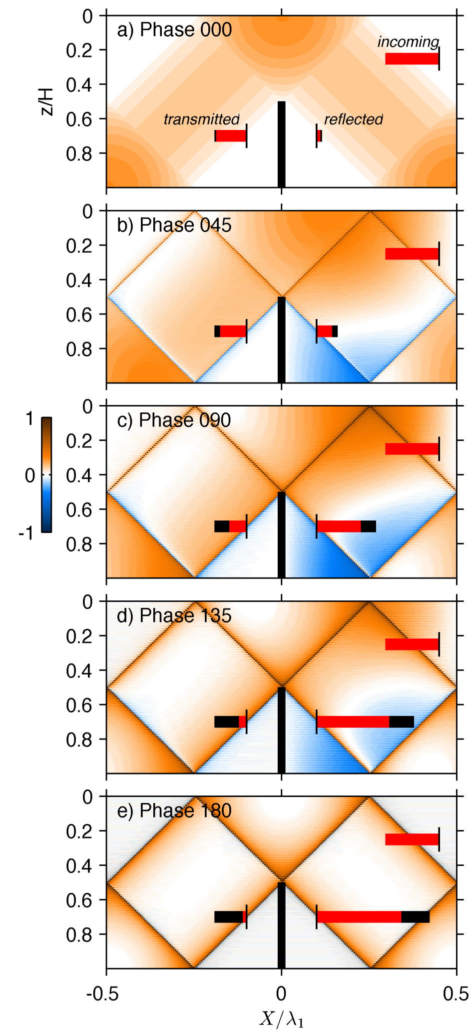

FIG. 8. Velocity snapshots for a barotropic tide of amplitude 0.1 $\mathrm{m\,s^{-1}}$ interacting with a mode-1 tide of amplitude 0.1 $\mathrm{m\,s^{-1}}$, with five different phase differences between the two tides. Here $h/H = 0.6$, and the stratification is constant. The energy flux is indicated in each panel as the black and red bars, with red indicating mode-1 energy, and black indicating all the energy. The incoming flux is plotted atop the ridge, and the reflected to the right, and the transmitted to the left. For each case, the incoming internal energy is the same, but the transmitted and reflected vary substantially.

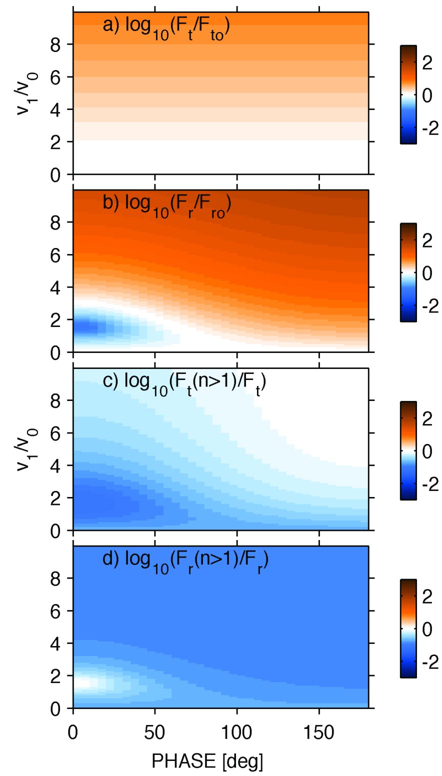

Fig. 9. Energy flux partition for mode-1 tide with amplitude v_1, and a barotropic tide with amplitude v_0 for different phase differences over a ridge with $h/H = 0.6$. a) Transmitted flux normalized by the barotropic-only flux. b) Reflected flux normalized by the barotropic-only right-going flux. c) Fraction of transmitted flux in high modes ($n > 1$). d) Fraction of reflected flux in high modes.

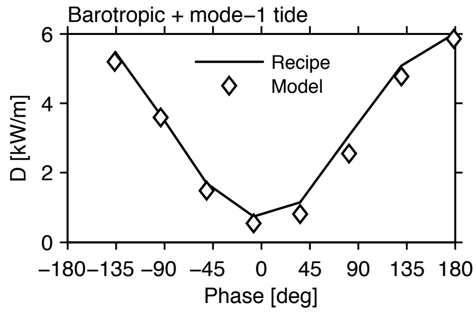

FIG. 10. Comparison of theoretical dissipation (solid line), and dissipation observed in model (symbols), for a ridge with $h/H = 0.6$, $v_0 = 0.1\ \mathrm{m\,s^{-1}}$, and $v_1 = 0.11\ \mathrm{m\,s^{-1}}$.

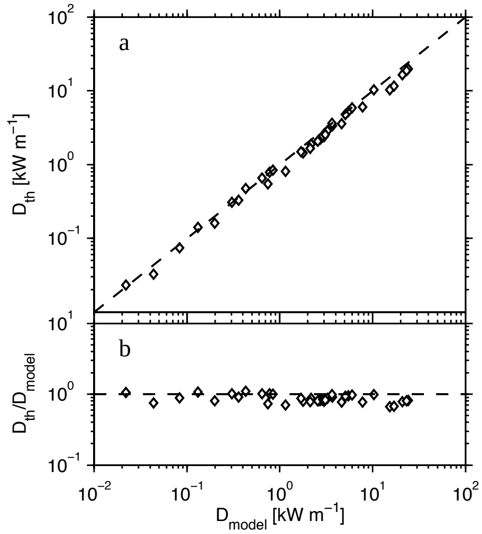

FIG. 11. Comparison of the recipe dissipations D_{th} and the numerical model dissipations D_{model}. Runs here were made with $h/H = 0.6$, and eight combinations of v_0, v_1, as described in TABLE 2.

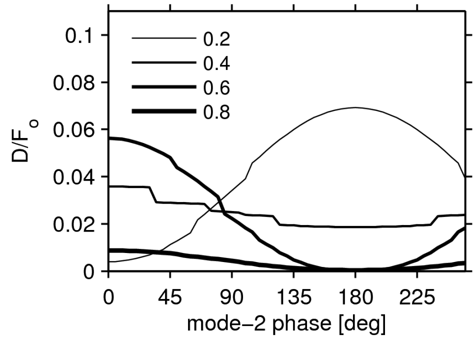

FIG. 12. Dissipation predicted from the recipe for an internal tide consisting of both mode-1 and mode-2 waves with equal amplitudes impacting a ridge, presented as a function of the phase between the mode-1 and mode-2 tides when they arrive at the ridge crest. The four curves represent four different ridges heights.

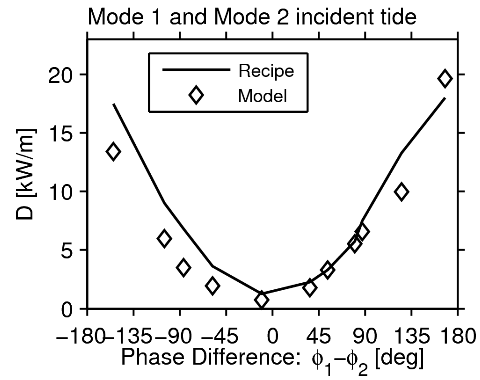

FIG. 13. Comparison of recipe dissipation and numerical model dissipation for a mode-1 and mode-2 incoming internal tide impinging on a knife edge with $h/H = 0.25$, and both mode-1 and mode-2 having amplitudes of 0.55 $\mathrm{m\,s^{-1}}$, but being forced at varying phases.

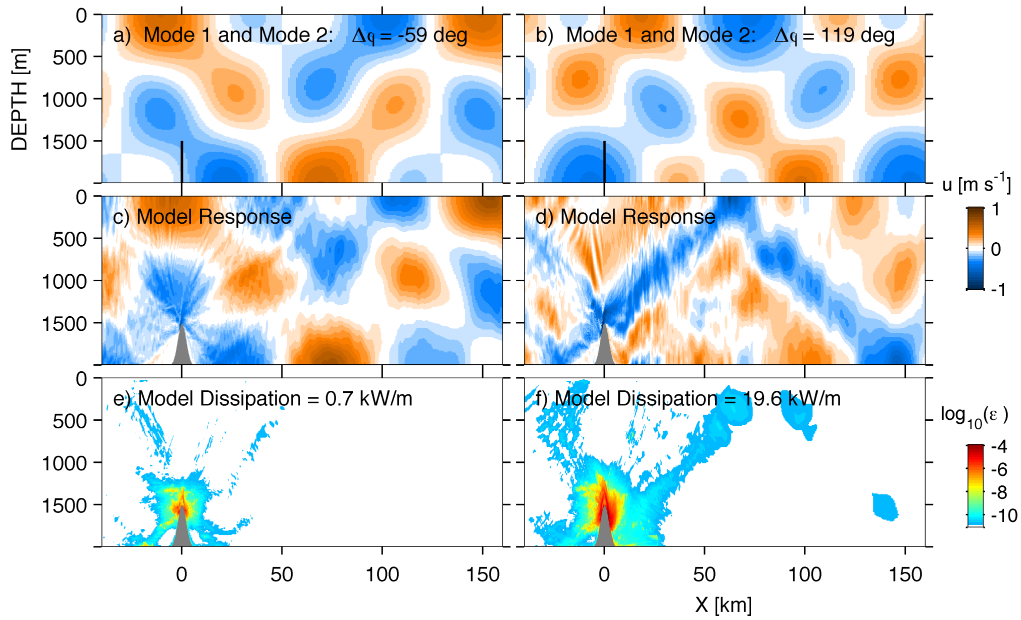

FIG. 14. a) and b) Velocity snapshots of the specified forcing from an incoming mode-1 and mode-2 tides (reflection and actual transmission not shown). c) and d) the response from the numerical model, and e) and f) the tidal-averaged dissipation at the ridge. Note the higher dissipation when the sum of the energy impacts the ridge crest.

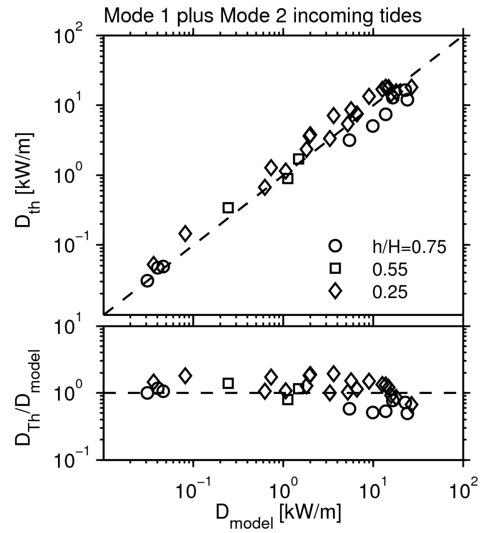

FIG. 15. Comparison of knife edge tidally-averaged dissipation (D_{th}), and numerical model dissipation (D_{model}) for a number of runs with mode-1 and mode-2 combined incoming fluxes at varying phase differences between the incoming waves.

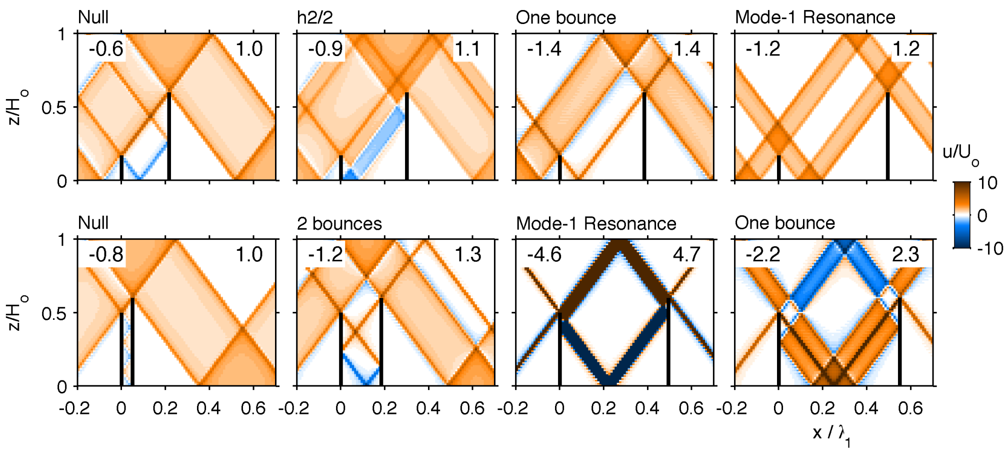

FIG. 16. a)–d) Velocity snapshots of the linear response of a two-ridge forcing if the two ridges are such that $h_1 + h_2 < H$, or e)–h) $h_1 + h_2 > H$ (lower row). The velocity is scaled by the barotropic velocity amplitude. The number in the left hand corner of each panel is the energy flux to the left, scaled by the energy flux that the same barotropic forcing would give if the topography was only comprised of the right-hand ridge. The number on the right is scaled energy flux to the right. The case with $h_1 + h_2 > H$ has a resonance when the ridges are half a mode-1 wavelength apart.

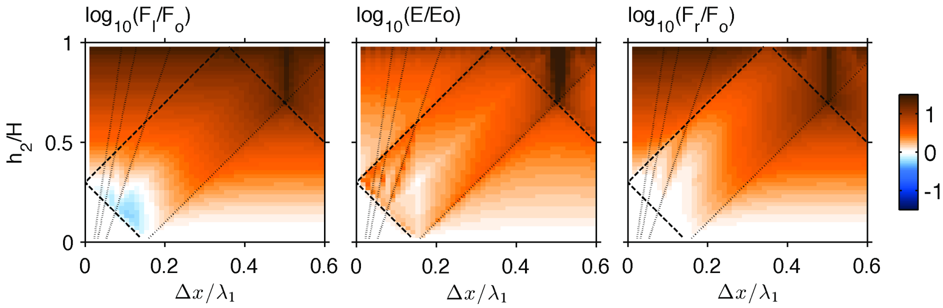

FIG. 17. Response of a two-ridge system with the right-side ridge held at a constant height $h_1 = 0.6H$, and the left hand ridge height varied, and the spacing between the ridges varied as $\Delta x/\lambda_1$, where λ_1 is the mode-1 horizontal wavelength. a) Is energy flux to the left, b) is the energy density between the ridges, and c) the energy flux to the right.

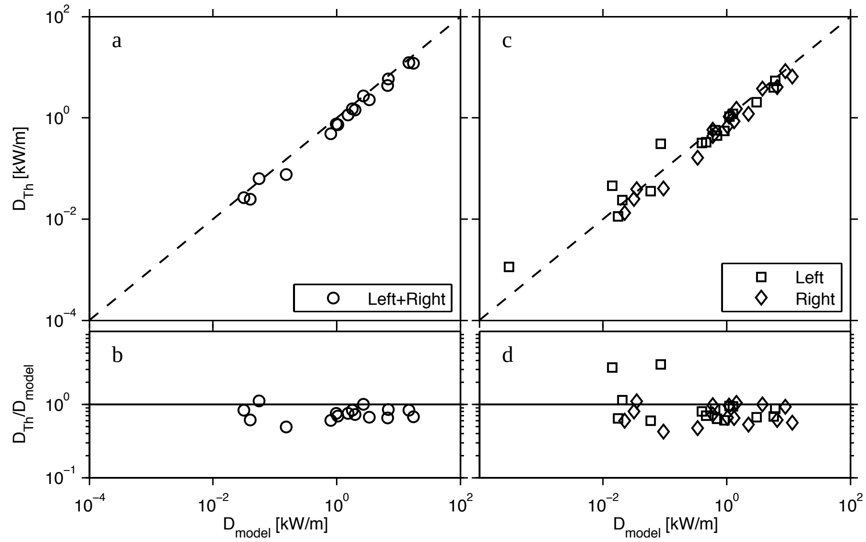

FIG. 18. Model versus "theory" tests for the two-ridge system. This was for two ridges, one with $h_l/H = 0.17$, and the other with $h_r/H = 0.60$. The strength of the forcing was varied, as was the distance between the ridges. a-b) the total dissipation of the system; c-d) the dissipation at the individual ridges.

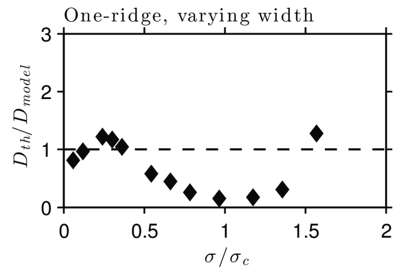

FIG. 19. Effect of widening the ridge on the dissipation predicted from a mode-1 incoming tide impinging on ridge with $h/H = 0.6$, and the tidal amplitude of 0.25 $\mathrm{m\,s^{-1}}$. The critical width is given by the slope of the internal tidal rays; as the topography gets shallower than $0.5w_c$ the model response increases significantly, and the theory under-predicts the numerical results.

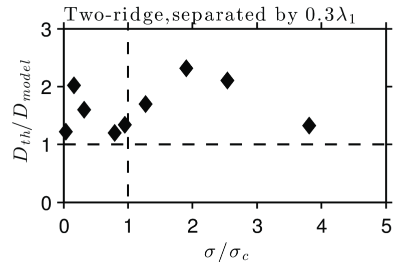

FIG. 20. Two-ridge case, $h_1/H = 0.17$, and $h_2/H = 0.6$, separated by $\Delta x/\lambda_1 = 0.3$. The critical width is compared to the height of the large ridge.

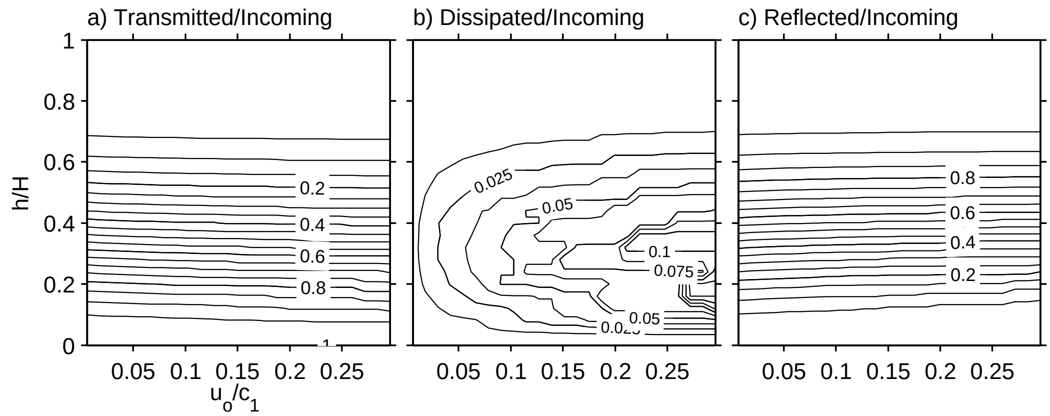

FIG. 21. Transmission, dissipation and reflection for a mode-1 wave impacting an isolated ridge, as predicted by the recipe in this paper. The amplitude of the mode-1 wave u_o is normalized by the mode-1 wave speed, $c_1 = 3.3\ \mathrm{m\,s^{-1}}$.

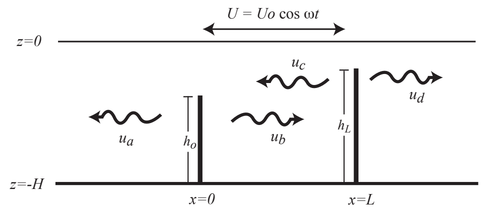

FIG. 22. Setup of the general two-ridge problem, including a barotropic tide, and an incoming internal wave from the right hand side.